Aust. J. Phys., 1996, **49**, 445–56

Excited-state Structure and Dynamics of Nitric Oxide probed by Resonant Four-wave Mixing Techniques*

E. F. McCormack,[A] *S. T. Pratt, P. M. Dehmer and J. L. Dehmer*

Argonne National Laboratory, Building 203,
9700 South Cass Avenue, Argonne, IL 60439, USA.
[A] Present address: Department of Physics,
Bryn Mawr College, Bryn Mawr, PA 19010-2899, USA.

Abstract

We review the results from two experiments that used resonant four-wave mixing (RFWM) techniques to investigate double-resonance transitions in NO. In the first experiment, laser-induced grating decay curves that reveal quantum beats due to the hyperfine structure of the $A\,^2\Sigma, v' = 0$ state were observed and interpreted. In the second, multistate interactions between the $L\,^2\Pi_{1/2,3/2}, v = 8$ and $Q\,^2\Pi_{1/2,3/2}, v = 0$ states were investigated, and new assignments were made. The results highlight the potential of RFWM techniques for probing excited-state physics.

1. Introduction

Resonant four-wave mixing (RFWM) techniques continue to be developed as effective nonlinear optical probes of both stable and transient atomic and molecular species. Examples include degenerate four-wave mixing (DFWM), where all input fields are tuned to a single transition frequency, and two-colour RFWM, where two input frequencies, resonant with two distinct transitions, are used. The signal in RFWM can be viewed as the formation of and the diffraction from laser-induced gratings. The grating picture is a particularly useful characterisation in the case of two-colour RFWM, where a distinction in frequency and time can be made between the grating-forming transition and the probe transition. Hence, two-colour RFWM is often referred to as laser-induced grating spectroscopy (LIGS).

The oldest and best known applications of DFWM and LIGS are in the area of optical phase conjugation (Fisher 1983) and in the measurement of ultrafast relaxation processes in liquids and solids (Eichler *et al.* 1986; Fourkas and Fayer 1992). DFWM was first demonstrated in the gas phase for sodium atoms in the late 1970s (Bloom *et al.* 1978). Soon thereafter, the detection of molecular species was also demonstrated; a review of this application of DFWM was given by Farrow and Rakestraw (1992, and references therein). DFWM gained additional interest as a method suitable for hostile environments when Ewart and O'Leary (1986) demonstrated that it could be used as an effective diagnostic of flames. Since that time, the technique has played a significant role in combustion research

* Refereed paper based on a contribution to the Advanced Workshop on Atomic and Molecular Physics, held at the Australian National University, Canberra, in February 1995.

0004-9506/96/020445$05.00

(Lucht *et al.* 1993, and references therein), and it has been used to characterise reacting plasmas (Green *et al.* 1993). Most recently, infrared DFWM has been used to study rovibrational transitions in molecules (Germann *et al.* 1995; Dreizler *et al.* 1995).

RFWM methods have begun to be applied to background-free, state-selective, two-colour schemes in order to explore the full potential of DFWM and LIGS. For example, DFWM has been used to perform background-free transition detection in stimulated-emission spectroscopy (Zhang *et al.* 1992; Vaccaro 1994). Two-colour LIGS has been demonstrated in free jets (Butenhoff and Rohlfing 1992) and used in double-resonance spectroscopy of many stable (Buntine *et al.* 1992, 1995; McCormack *et al.* 1993, 1994, 1995; Butenhoff and Rohlfing 1993*a*; Dunlop and Rohlfing 1994; Wheeler *et al.* 1993) and transient species (Gray *et al.* 1993; Williams *et al.* 1994*a*, 1995; Butenhoff and Rohlfing 1992). In addition to spectroscopy, the time evolution of the transient gratings produced in LIGS has been used as a powerful method to probe inter- and intramolecular dynamics (Rose *et al.* 1987). A recent example of this application in the gas phase was the use of transient gratings to determine the velocity distribution of very slow NO fragments produced in the near-threshold photodissociation of NO_2 (Butenhoff and Rohlfing 1993*b*).

The DFWM and LIGS techniques have several advantages over other spectroscopic methods. Unlike fluorescence-dip spectroscopy, which has traditionally been used to obtain excited-state absorption spectra or stimulated-emission spectra, the DFWM and LIGS techniques produce a zero-background signal and do not require the state of interest to fluoresce. Further, the DFWM and LIGS techniques can have sub-Doppler resolution, and the signal is a coherent beam that travels in a well-defined direction. These appealing attributes make DFWM and LIGS effective tools for performing excited-state spectroscopy and dynamics. In this paper, we highlight the potential of LIGS for probing excited-state physics by reviewing the results of two double-resonance experiments on NO using two-colour LIGS via the $A\,^2\Sigma, v' = 0$ state. Both experiments have been described previously in detail (McCormack *et al.* 1994, 1995).

2. Experiment

The LIGS technique is based on a type of resonant four-wave mixing process that, in many cases, can be described simply by light-induced gratings (Eichler *et al.* 1986). With this technique, two laser beams crossed at a small angle in a medium, interfere to produce a sinusoidal modulation of light intensity. When the wavelength is tuned to a transition in the sample, the varying light intensity produces alternating regions of excited and ground-state populations. These alternating regions result in a Bragg diffraction grating characterised by a varying absorption coefficient and index of refraction. In this case the grating is called a population grating, because it arises from a population transfer due to excitation caused by the grating-forming laser beam. However, any interaction of the light with the sample that results in a spatial variation in the complex index of refraction will produce a grating. Other examples include density gratings and polarisation gratings. A LIGS signal is produced by scattering a third laser beam, the probe, off this grating to produce a fourth beam which propagates

in a unique, well-defined direction. The four-wave-mixing process is strongly enhanced when the frequency of the light corresponds to a molecular transition because of the resonant behaviour of the third-order nonlinear susceptibility χ^3 of the sample. Thus, monitoring the wavelength dependence of the LIGS signal beam allows a spectrum of the sample molecule to be obtained. Further, the time evolution of the grating, which reflects both properties of the environment of the sample and properties of the sample transitions involved in the grating formation, can be studied by varying the delay between the grating-forming laser pulses and the probe laser pulse.

Fig. 1 shows a schematic diagram of the experimental arrangement used to study NO. Light at ~226 nm, which was used to excite the $A^2\Sigma$, $v' = 0, J' \leftarrow X\,^2\Pi_{1/2}$, $v'' = 0, J''$ grating transitions, was generated by frequency doubling the output of a pulsed Nd:YAG-pumped dye laser. Light at ~412 nm, which was used to excite the $B\,^2\Pi_{1/2,3/2}$, $v = 28$; $L\,^2\Pi_{1/2,3/2}$, $v = 8$; and $Q\,^2\Pi_{1/2,3/2}$, $v = 0, J \leftarrow A\,^2\Sigma$, $v' = 0$, J' probe transitions, was produced by a second pulsed Nd:YAG-pumped dye laser. The pulses from the two lasers were ~8 ns in duration, and all laser beams were collimated to a diameter of ~2 mm. The bandwidth of both the 226-nm light and the 412-nm light was $\sim 0{\cdot}4\ \mathrm{cm}^{-1}$. The wavelength of the laser light at 412 nm was calibrated by recording the optogalvanic spectra of neon and uranium simultaneously with the LIGS spectrum.

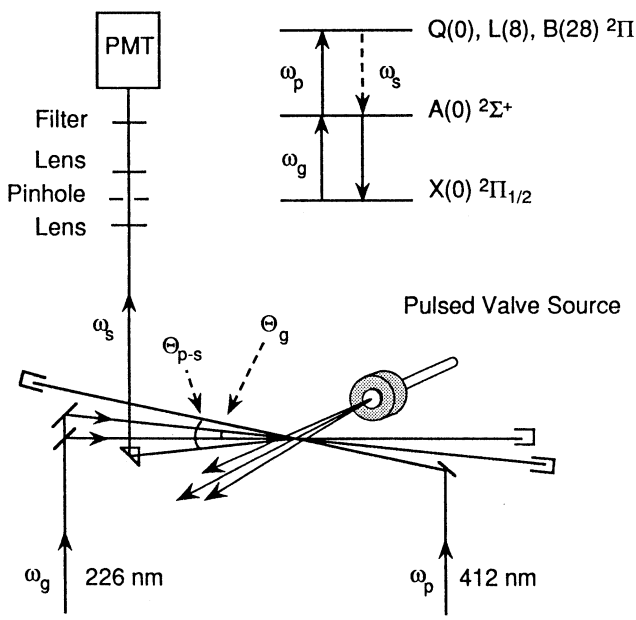

Fig. 1. Experimental arrangement for LIGS using a pulsed jet source.

A molecular beam was produced by a pulsed valve operated with a backing pressure of ~1 atmosphere of pure NO ($\equiv$101·33 kPa). Laser light at 226 nm, with $\omega_g = 2\pi c/\lambda_g$, was divided into two beams that were crossed at a small angle ($\theta_g = 3°$) in the interaction region to form the grating. Probe light at 412 nm,

ω_p, was then scattered off the grating to produce the signal beam ω_s. The angle of incidence for the probe beam is restricted by the phase-matching constraint, equivalent to the Bragg scattering condition $\lambda_g/\sin(\theta_g/2) = \lambda_p/\sin(\theta_{p-s}/2)$ (Eichler *et al.* 1986). The signal beam was detected through a spatial filter consisting of a telescope and pinhole; a colour filter was used to further reduce background due to scattered light.

For the results presented here, the polarisations of the grating-forming laser pulses were always parallel to one another, but they could be rotated with respect to the polarisation of the probe laser pulses by using a double rhomb. A polariser in the path of the signal beam was used to selectively observe the polarisation of the generated LIGS signal in a direction either parallel or perpendicular to the probe polarisation. The major velocity component of the molecular beam was arranged to be perpendicular to the grating wave vector $\boldsymbol{k}_g = \boldsymbol{k}_{g1} - \boldsymbol{k}_{g2}$ or, equivalently, parallel to the grating fringes. In this way the decay of the grating due to molecular motion was reduced from that for a room temperature sample (~10 ns) to that given by the residual transverse velocity distribution of the molecules in the beam, which in a jet expansion is quite small.

Throughout our discussion, levels of the $X\,^2\Pi_{1/2}$, $v'' = 0$ state are denoted with double primes, levels of the $A\,^2\Sigma$, $v' = 0$ state are denoted with single primes, and levels of the $B\,^2\Pi_{1/2,3/2}$, $v = 28$, $L\,^2\Pi_{1/2,3/2}$, $v = 8$ and $Q\,^2\Pi_{1/2,3/2}$, $v = 0$ states are denoted without primes. In addition, a shorthand notation for the vibrational quantum number is used; for example, $B\,^2\Pi_{1/2}$, $v = 28$ is denoted $B(28)\,^2\Pi_{1/2}$.

3. Results and Discussion

(3a) *Multistate Interactions in NO*

The LIGS techniques provide a valuable complement to decay-dependent detection schemes, because they are sensitive to transitions regardless of the mode of decay of the final state. This is demonstrated in Fig. 2, which compares fluorescence-dip detection (top frame), resonant multiphoton ionisation (MPI) detection (middle frame), and two-colour LIGS detection (bottom frame) of the $B(28)\,^2\Pi_{1/2,3/2}$, $J \leftarrow A(0)\,^2\Sigma$, J' probe transition in NO. Note that the $\Omega = \frac{3}{2}$ component of the $B\,^2\Pi$ state has a very short (~10 ps) lifetime (Ebata *et al.* 1983). The spectrum obtained by using fluorescence-dip detection (top frame) provides direct information on the absorption cross section of the intermediate $A(0)\,^2\Sigma$ state; the cross sections for populating the $\Omega = \frac{1}{2}$ and $\frac{3}{2}$ spin components of the $B\,^2\Pi_\Omega$ state are approximately equal. However, the spectrum obtained by using photoionisation detection (middle frame) fails to show the true intensity of the transition to the $\Omega = \frac{3}{2}$ spin component of the $B\,^2\Pi$ state, because this component decays before it can be photoionised. The spectrum obained by using two-colour LIGS detection (bottom frame) shows both Ω components of the $B\,^2\Pi_\Omega$ state; furthermore, the signal-to-noise ratio of this spectrum is far superior to that in either of the other two spectra.

This ability of LIGS to detect transitions independent of the mode of decay of the excited state was critical in our recent study of the multistate interactions between the $L(8)\,^2\Pi_{1/2,3/2}$ and $Q(0)\,^2\Pi_{1/2,3/2}$ states of NO. Previous analysis

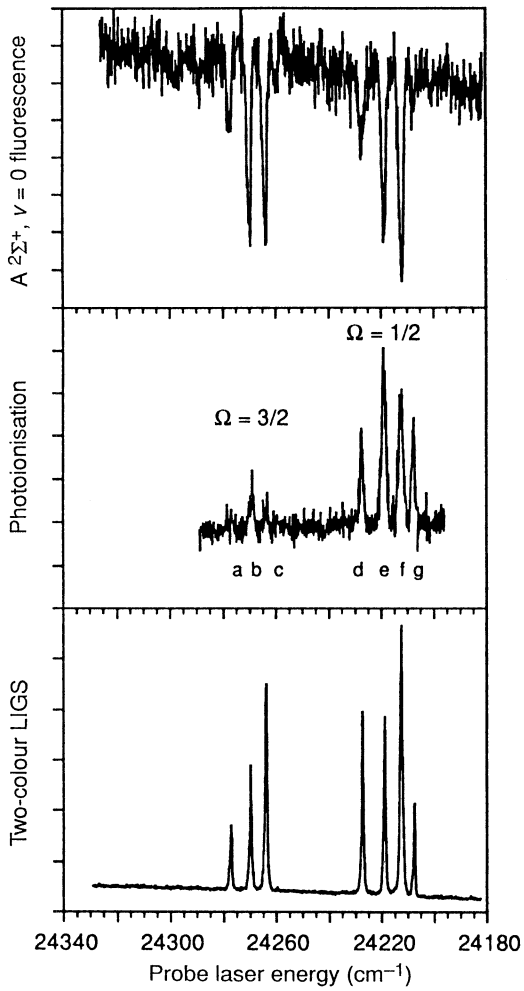

Fig. 2. Comparison of spectra obtained for a region of the two-colour B(28) $^2\Pi \leftarrow$ A(0) $^2\Sigma^+ \leftarrow$ X(0) $^2\Pi_{1/2}$ transition by using three detection techniques. Top frame: fluorescence-dip spectrum obtained by exciting the $^RQ_{21}(2{\cdot}5)+R_{11}(2{\cdot}5)$ branch of the A(0) $^2\Sigma^+ \leftarrow$ X(0) $^2\Pi_{1/2}$ transition and monitoring the induced A(0) $^2\Sigma^+$ state fluorescence while the probe laser is scanned. Middle frame: multiphoton ionisation spectrum obtained by exciting the same A(0) $^2\Sigma^+ \leftarrow$ X(0) $^2\Pi_{1/2}$ transition as above and monitoring the production of NO^+ ions via multiphoton absorption while the probe laser is scanned. Bottom frame: two-colour LIGS spectrum obtained by tuning the grating-forming lasers to the same A(0) $^2\Sigma^+ \leftarrow$ X(0) $^2\Pi_{1/2}$ transition as above and monitoring the laser-induced grating signal while the probe laser is scanned. The transitions shown are: a, $^SR_{21}(3{\cdot}5)$; b, $R_{22}(2{\cdot}5)+^RQ_{21}(3{\cdot}5)$; c, $Q_{22}(2{\cdot}5)+^OP_{21}(3{\cdot}5)$; d, $R_{11}(3{\cdot}5)$; e, $Q_{11}(3{\cdot}5)+^QR_{12}(2{\cdot}5)$; f, $P_{11}(3{\cdot}5)+^PQ_{12}(2{\cdot}5)$; and g, $^OP_{12}(2{\cdot}5)$.

of the multistate interactions between the L(8) $^2\Pi_{1/2,3/2}$ and Q(0) $^2\Pi_{1/2,3/2}$ states based on absorption (Dressler and Miescher 1965; Lagerqvist and Miescher 1966; Miescher and Huber 1976) and MPI studies (Ebata *et al.* 1983; Cheung *et al.* 1986) was hindered because in each of those studies only a fraction of the

transitions to the four interacting states was observed. The spectra obtained by using two-colour LIGS, however, revealed a complete set of transitions to the four states with exceptional signal-to-noise ratios. As a result, we made new assignments and reanalysed the interaction of the $L\,^2\Pi_{1/2,3/2}$, $v = 8$ and $Q\,^2\Pi_{1/2,3/2}$, $v = 0$ states. Below we give a summary of the results, which are described in detail in McCormack *et al.* (1995).

Two-colour LIGS of NO via the $A\,^2\Sigma$, $v' = 0$ state was used to investigate the energy region between 68400 and 68700 cm^{-1}, which includes transitions to the $B(28)\,^2\Pi_{1/2,3/2}$ and $L(8)\,^2\Pi_{1/2,3/2}$ valence states and the $Q(0)\,^2\Pi_{1/2,3/2}$ 5pπ Rydberg states. For the spectra shown in this section, all of the laser pulses were linearly polarised parallel to one another, and data were taken with the pulses from the two lasers overlapped in time. Several rotational levels of the $A(0)\,^2\Sigma^+$ state were used to probe transitions to the higher lying $B(28)\,^2\Pi_{1/2,3/2}$, $L(8)\,^2\Pi_{1/2,3/2}$ and $Q(0)\,^2\Pi_{1/2,3/2}$, states. These levels were reached by suitable choice of the $A(0)\,^2\Sigma^+$, $J' \leftarrow X(0)\,^2\Pi_{1/2}$, J'' grating transitions. Both the $A(0)\,^2\Sigma^+ \leftarrow X(0)\,^2\Pi_{1/2}$ and the $B(28)\,^2\Pi_{1/2,3/2}$ $L(8)\,^2\Pi_{1/2,3/2}$ and $Q(0)\,^2\Pi_{1/2,3/2}$, $\leftarrow A(0)\,^2\Sigma^+$ rotational branches are labelled as ${}^{\Delta N}\Delta J_{qr}(J)$, where ΔN is omitted for $\Delta N = \Delta J$. The q and r subscripts denote the spin component, F_1 or F_2, of the upper and lower states, respectively, and J is the total angular momentum of the lower state in the transition. The F_1 component has $J = N + \frac{1}{2}$, and the F_2 component has $J = N - \frac{1}{2}$. For a regular $^2\Pi$ state, such as the $B(28)\,^2\Pi_\Omega$ and the $Q(0)\,^2\Pi_\Omega$ states, the $\Omega = \frac{3}{2}$ level is higher in energy than the $\Omega = \frac{1}{2}$ level. For an inverted $^2\Pi$ state, such as the $L(8)\,^2\Pi_\Omega$ state, the $\Omega = \frac{3}{2}$ level is lower in energy than the $\Omega = \frac{3}{2}$ level.

Because the resolution of the spectra is limited by the laser bandwidth, both the spin- and Λ-splittings of the $A(0)\,^2\Sigma^+$ state and the Λ-splitting of the $X\,^2\Pi_{1/2}$ are unresolved at the J values probed here. This fact leads to the overlap of some branches in the $A(0)\,^2\Sigma^+ \leftarrow X(0)\,^2\Pi_{1/2}$ transition; for example, the $R_{11}(J'')$ and ${}^RQ_{21}(J'')$ branches are effectively degenerate. When overlapped branches of this type are used for the grating-forming transition, two levels of the $A(0)\,^2\Sigma^+$ state are populated, and probe transitions such as the $R_{22}(J')$ and ${}^RQ_{21}(J'+1)$ or $P_{11}(J')$ and ${}^PQ_{12}(J'-1)$ branches will appear degenerate. When this is the case, the transitions are labeled accordingly.

A representative spectrum obtained with the two-colour LIGS technique is shown in Fig. 3. In this example, the two-colour spectrum was obtained by fixing the grating laser, ω_g, on the $Q_{11}(0{\cdot}5)$ branch of the $A(0)\,^2\Sigma \leftarrow X(0)\,^2\Pi_{1/2}$ transition and scanning the probe laser across $B(28)\,^2\Pi_{1/2,3/2}$, $L(8)\,^2\Pi_{1/2,3/2}$ and $Q(0)\,^2\Pi_{1/2,3/2} \leftarrow A(0)\ \Sigma$, $J' = 0{\cdot}5$ transitions while the signal generated by the two-colour LIGS process was detected.

As a result of the spin-rotation interactions among the $Q(0)\,^2\Pi_{1/2,3/2}$ and $L(8)\,^2\Pi_{1/2,3/2}$ states, the electronic character of the observed states changes with increasing J. We use the notation T_x, T_y, T_z to denote the perturbed states in order of increasing energy in terms of the unperturbed states:

$$T_x: \quad Q(0)\,^2\Pi_{1/2} \rightarrow Q(0)\,^2\Pi_{1/2} \rightarrow L(8)\,^2\Pi_{1/2}\,,$$

$$T_y: \quad Q(0)\,^2\Pi_{3/2} \rightarrow L(8)\,^2\Pi_{1/2} \rightarrow Q(0)\,^2\Pi_{1/2}\,,$$

$$T_z: \quad L(8)\,^2\Pi_{1/2} \rightarrow Q(0)\,^2\Pi_{3/2} \rightarrow Q(0)\,^2\Pi_{3/2}\,,$$

and

$$T_x < T_y < T_z\,.$$

Here $\rightarrow$ denotes the character change with increasing J. The $L(8)\,^2\Pi_{1/2}$ and $Q(0)\,^2\Pi_{3/2}$ states cross at $J \sim 1{\cdot}5$–$2{\cdot}5$, and the $L(8)\,^2\Pi_{1/2}$ and $Q(0)\,^2\Pi_{1/2}$ states cross at $J \sim 5{\cdot}5$–$6{\cdot}5$. The $L(8)\,^2\Pi_{3/2}$ state lies at a lower energy, well separated from the other states; therefore, it does not cross any of the other states. At low J, the assignment of the upper levels of the observed transitions to the Q, L states is ambiguous, as is the assignment to the F_1 or F_2 component, and only the J value and total parity can be assigned rigorously. However, at high J, because of spin uncoupling, the states can be identified as $L(8)\,^2\Pi_{1/2,3/2}$ and $Q(0)\,^2\Pi_{1/2,3/2}$ states (neglecting angular momentum-rotation uncoupling).

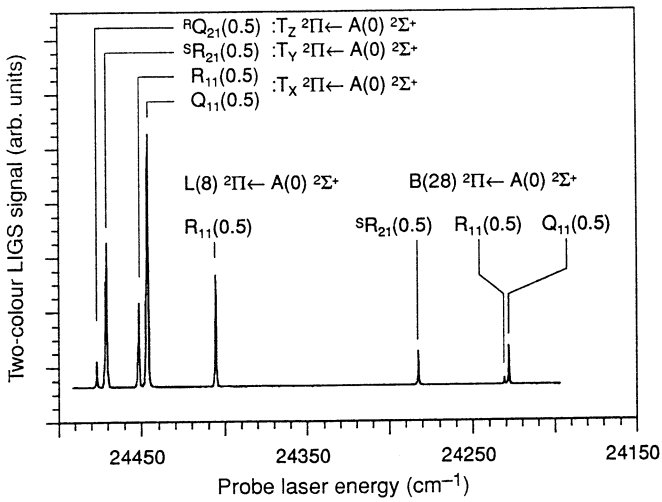

Fig. 3. Two-colour LIGS spectrum obtained by tuning the grating-forming lasers to the $Q_{11}(0{\cdot}5)$ branch of the $A(0)\,^2\Sigma^+ \leftarrow X(0)\,^2\Pi_{1/2}$ transition and scanning the probe laser in the energy regime of several $Q(0)\,^2\Pi_{1/2,3/2}$ and $L(8)\,^2\Pi_{1/2,3/2}$ rotational levels—see text for an explanation of the state labels.

The term energies for the $B(28)\,^2\Pi_{1/2,3/2}$ states and the T_x, T_y, T_z and $L(8)\,^2\Pi_{3/2}$ states are plotted as a function of $J(J{+}1)$ in Fig. 4. Energies are plotted relative to the $X\,^2\Pi_{1/2}$, $v'' = 0$, $J'' = \frac{1}{2}$ level of the ground state; they were obtained by adding the appropriate $A\,^2\Sigma$, $v' = 0$, J' term energies (Amiot and Verges 1982). Transition energies and term energies are tabulated in McCormack *et al.* (1995).

The interaction between the $L(8)\,^2\Pi_{1/2,3/2}$ and $Q(0)\,^2\Pi_{1/2,3/2}$ states has been known experimentally since the work of Dressler and Miescher (1965). They observed transitions from the ground state to the T_x state in absorption and were able to deduce the presence of at least one other state in the interaction

on the basis of the J-dependent behaviour of the levels. Double-resonance MPI studies via the A(1) $^2\Sigma^+$ intermediate state revealed transitions to levels of both the L(8) $^2\Pi_{3/2}$ state and the T_y state (Cheung *et al.* 1986), as well as several weaker transitions to levels of the T_z state (Raoult 1987). However, transitions to levels of the T_x state, seen in absorption, were not observed in the MPI study. By using two-colour LIGS, all four of the T_x, T_y, T_z and L(8) $^2\Pi_{3/2}$ states were observed for the first time in one experiment.

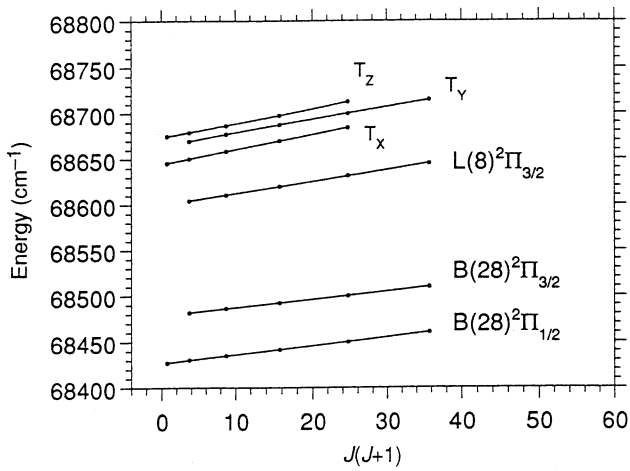

Fig. 4. Plot of term values versus $J(J+1)$. Experimental data are shown as points. The lines are the results of linear fits to data for the T_x, L(8) $^2\Pi_{3/2}$, B(28) $^2\Pi_{1/2}$ and B(28) $^2\Pi_{1/2}$ levels. The lines for the T_y and T_z levels connect a cubic spline fit to the results of the two-state deperturbation analysis of these levels. See McCormack *et al.* (1995) for details.

As a result, we have made new assignments and reconsidered the interaction of the L $^2\Pi_{1/2,3/2}$, $v = 8$ and Q $^2\Pi_{1/2,3/2}$, $v = 0$ states. The details of our deperturbation analysis and rotational constants are given in McCormack *et al.* (1995). Clarification of the interpretation of the low J levels is important because the analysis of the $^2\Pi$–$^2\Pi$ Rydberg-valence state interactions of NO is sensitive to the L $^2\Pi$ state potential energy curve, which is determined from experimental energies. The $v = 8$ level is key to this determination, because measurements for both the $\Omega = \frac{1}{2}$ and $\frac{3}{2}$ levels are available. The new assignments are expected to give a more accurate L $^2\Pi$ state potential energy curve and result in better agreement between the theoretical models (Gallusser and Dressler 1982; Raoult 1987) and experiment.

(3b) Time-resolved LIGS: Hyperfine Quantum Beats

In the second experiment, two-colour LIGS in a supersonic molecular beam was used to study the time evolution of laser-induced gratings in NO. By varying the delay between the grating-forming laser pulse and the grating-probing laser pulse, we observed quantum beats due to the hyperfine structure of the A $^2\Sigma^+$, $v' = 0$ state in the LIGS signal for specific polarisation configurations of the input laser beams (McCormack *et al.* 1994). Depending on the polarisation configuration,

the two-colour LIGS signal either decayed monotonically as a function of probe delay, reflecting residual motion in the molecular beam and the lifetime of the grating-forming state, or showed oscillatory behaviour as a function of the delay of the probe laser in addition to the smooth decay. The observed periodicity in the oscillations and the dependence on polarisation indicate that the oscillations are a type of quantum beat due to coherent excitation of multiple hyperfine levels of the $A\,^2\Sigma^+$, $v' = 0$ state that lie within the laser bandwidth.

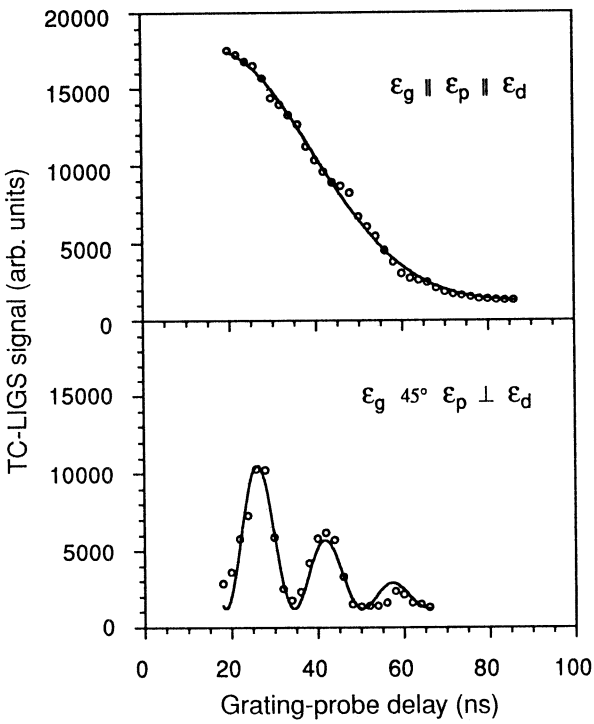

Fig. 5. Two-colour LIGS signal as a function of the delay between the grating-forming laser pulses and the probe laser pulse. The lasers are tuned to the $L\,^2\Pi_{3/2}, J = 1{\cdot}5,\ v = 8 \leftarrow A\,^2\Sigma, J' = 0{\cdot}5, v' = 0 \leftarrow X\,^2\Pi_{1/2}, J'' = 0{\cdot}5, v'' = 0$ transition. Data are shown as open circles and fits are shown as curves. See McCormack *et al.* (1994) for details on the fits.

Grating decay curves were obtained by tuning the wavelength of the grating and probe lasers to a particular two-colour LIGS double-resonance transition and then varying the time delay between the grating-forming laser pulses and the probing laser pulse. Two such curves for the $L\,^2\Pi_{3/2}, J = 1{\cdot}5,\ v = 8, \leftarrow A\,^2\Sigma, J' = 0{\cdot}5, v' = 0 \leftarrow X\,^2\Pi_{1/2}, J'' = 0{\cdot}5, v'' = 0$ transition are shown in Fig. 5. Each decay curve was obtained with a distinct polarisation configuration. The top frame in Fig. 5 shows the curve obtained with the polarisation of the grating-forming laser pulses ϵ_g and the probe laser pulse ϵ_p parallel to one another and with the detection polariser in the signal beam path ϵ_d configured to allow light polarised parallel to the probe laser pulse to pass. No signal is observed with ϵ_d perpendicular to ϵ_p. This curve exhibits a smooth monotonic decrease

in signal as the delay between the grating-forming laser pulses and the probe laser pulse is increased. The bottom frame in Fig. 5 shows the curve obtained for ϵ_p rotated 45° with respect to ϵ_g and ϵ_d set perpendicular to ϵ_p. With this polarisation configuration, the two-colour LIGS signal exhibits a marked oscillation in intensity as a function of the probe pulse delay. The contrast in the oscillatory component of the signal is maximised when the polarisations of the grating and probe pulses are rotated 45° with respect to each other. Further, only the component of the signal polarised perpendicular to the probe laser shows the oscillatory structure; the component of the signal polarised parallel to the probe laser shows a smooth decay curve similar to the upper frame in Fig. 5.

The overall monotonic grating decay observed in Fig. 5 is due to two factors: the lifetime of the intermediate $A\,^2\Sigma^+, v' = 0$ state and the residual transverse motion in the molecular beam. An analysis of these effects is given in McCormack *et al.* (1994). The oscillatory behaviour in the grating decay curve shown in the bottom frame of Fig. 5 is due to the coherent excitation of multiple molecular hyperfine levels of NO. The two grating-forming pulses coherently excite the hyperfine levels of the $A\,^2\Sigma^+$, $v = 0$ state that lie within the laser bandwidth. The grating-forming laser pulses produce anisotropic contributions to the molecular absorption in the form of nonuniform magnetic level populations in the ground and excited states. The time evolution of the coherent superposition of states causes the anisotropic contributions to oscillate in time. The oscillating anisotropic contributions to the grating are selectively observed by scattering off the grating probe light with a polarisation rotated 45° with respect to the grating-forming light pulses, then detecting the scattered signal through a polariser rotated 90° with respect to the polarisation of the probe light pulse.

The oscillations are a type of quantum beat with a frequency equal to the energy separation between two coherently excited levels. Accordingly, the oscillation period of 15·8 ns agrees well with the expected energy separation between the $F' = 1{\cdot}5$ and $0{\cdot}5$ hyperfine levels of the $A\,^2\Sigma^+, v' = 0, J' = 0{\cdot}5$ state, on the basis of the energy separation observed, 62·1 MHz, for the equivalent states in the $v' = 1$ level (McCormack *et al.* 1994). Remarkaby, this measured energy separation is smaller by more than two orders of magnitude the bandwidth of the nanosecond pulsed lasers used. This dramatic improvement in energy resolution with the use of conventional pulsed lasers is typical of quantum beat spectroscopic techniques (Bitto and Huber 1992), but the quantum beats discussed here have several distinct advantages inherent to LIGS, including background-free detection, two-colour state selectivity, a quadratic dependence on the level population, and a beat signal independent of the decay mode of the state.

(*3c*) *Theoretical Considerations*

The ability to characterise the intensities in two-colour LIGS so that true absorption cross sections can be obtained from spectra is necessary for quantitative measurements. Toward this end, a description of two-colour LIGS based on an extension of work on DFWM (Williams *et al.* 1994*b*) that combines time-independent diagrammatic perturbation theory with spherical tensor analysis has very recently been developed and applied to measurements of intensities and line shapes in two-colour RFWM experiments on C_3 and HCO (Williams *et al.*

1995). These methods look very promising for quantitative interpretation of line intensities observed by using typical experimental arrangements and a variety of polarisation configurations.

A detailed description of time-resolved, polarisation-selective, RFWM that incorporates coherent excitation of hyperfine levels in molecules in the gas phase is necessary for a complete interpretation of the hyperfine beats discussed above. Time-dependent theories that use a density matrix formalism have been developed and used in condensed-phase studies. Various examples are discussed in the review by Deeg and Fayer (1989). More recently, a grating decomposition method (GDM) has been developed and used to explain observations of nuclear optical Kerr effects and ground-state hyperfine beats in polarisation grating experiments (Fourkas *et al.* 1992). Either the GDM or density matrix approach should be capable of describing the molecular hyperfine quantum beats we have observed.

4. Conclusions

Nonlinear optical techniques continue to be developed and applied as new probes in atomic and molecular spectroscopy. The RFWM techniques have the potential for sensitive, selective detection of stable and transient species and offer certain advantages over traditional techniques like fluorescence-dip and resonant ionisation spectroscopy for studying excited-state structure and dynamics in atoms and molecules. We have used several RFWM techniques, including DFWM and LIGS, to study double-resonance transitions in NO. The results from two experiments have been reviewed.

Two-colour LIGS of NO via the $A\,^2\Sigma$, $v' = 0$ state was used to investigate the energy region between 68400 and 68700 cm^{-1}, which includes transitions to the $B\,^2\Pi_{1/2,3/2}$, $v = 28$ and $L\,^2\Pi_{1/2,3/2}$, $v = 8$ valence states and the $Q\,^2\Pi_{1/2,3/2}$, $v = 0$ $5p\pi$ Rydberg states (McCormack *et al.* 1995). The spectra obtained by using two-colour LIGS revealed a complete set of transitions to the $L\,^2\Pi_{1/2,3/2}$, $v = 8$ and $Q\,^2\Pi_{1/2,3/2}$, $v = 0$ states with exceptional signal-to-noise ratios. As a result, new assignments were made, and the multistate interactions between the $L\,^2\Pi_{1/2,3/2}$, $v = 8$ and $Q\,^2\Pi_{1/2,3/2}$, $v = 0$ states were reexamined.

In addition, two-colour LIGS in a supersonic molecular beam was used to study the time evolution of laser-induced gratings in NO (McCormack *et al.* 1994). By varying the delay between the grating-forming laser pulse and the grating-probing laser pulse, quantum beats due to the hyperfine structure of the $A\,^2\Sigma^+$, $v' = 0$ state were observed in the LIGS signal for specific polarisation configurations of the input laser beams. Compared to traditional fluorescence quantum beat spectroscopy, this new form of nonlinear quantum beat spectroscopy has the advantages of background-free detection, two-colour state selectivity, a quadratic dependence on the level population, and a beat signal independent of the decay mode.

Acknowledgments

Supported by the US Department of Energy, Office of Energy Research, under Contract W-31–109-ENG-38.

References

Amiot, C., and Verges, J. (1982). *Phys. Scripta* **26**, 422.
Bitto, H., and Huber, J. R. (1992). *Acc. Chem. Res.* **25**, 65.
Bloom, D. M., Liao, P. F., and Economou, N. P. (1978). *Opt. Lett.* **2**, 58.
Buntine, M. A., Chandler, D. W., and Hayden, C. C. (1992). *J. Chem. Phys.* **97**, 707.
Buntine, M. A., Chandler, D. W., and Hayden, C. C. (1995). *J. Chem. Phys.* **102**, 2718.
Butenhoff, T. J., and Rohlfing, E. A. (1992). *J. Chem. Phys.* **97**, 1595.
Butenhoff, T. J., and Rohlfing, E. A. (1993*a*). *J. Chem. Phys.* **98**, 5460.
Butenhoff, T. J., and Rohlfing, E. A. (1993*b*). *J. Chem. Phys.* **98**, 5469.
Cheung, W. Y., Chupka, W. A., Colson, S. D., Gauyacq, D., Avouris, P., and Wynne, J. J. (1986). *J. Phys. Chem.* **90**, 1086.
Deeg, F. W., and Fayer, M. D. (1989). *J. Chem. Phys.* **91**, 2269.
Dreizler, A., Dreier, T., and Wolfrum, J. (1995). *Chem. Phys. Lett.* **233**, 525.
Dressler, K., and Miescher, E. (1965). *Astrophys. J.* **141**, 1266.
Dunlop, J. R., and Rohlfing, E. A. (1994). *J. Chem. Phys.* **100**, 856.
Ebata, T., Mikami, N., and Ito, M. (1983). *J. Chem. Phys.* **78**, 1132.
Eichler, H. J., Gunter, P., and Pohl, D. W. (1986). 'Laser-induced Dynamic Gratings' (Springer: Berlin).
Ewart, P., and O'Leary, S. V. (1986). *Opt. Lett.* **11**, 279.
Farrow, R. L., and Rakestraw, D. J. (1992). *Science* **257**, 1894.
Fisher, R. A. (Ed.) (1983). 'Optical Phase Conjugation' (Academic: New York).
Fourkas, J. T., and Fayer, M. D. (1992). *Acc. Chem. Res.* **25**, 2277.
Fourkas, J. T., Trebino, R., and Fayer, M. D. (1992). *J. Chem. Phys.* **97**, 69; 78.
Gallusser, R., and Dressler, K. (1982). *J. Chem. Phys.* **76**, 4311.
Germann, G. J., Farrow, R. L., and Rakestraw, D. J. (1995). *J. Opt. Soc. Am.* B **12**, 25.
Gray, J. A., Goldsmith, J. E. M., and Trebino, R. (1993). *Opt. Lett.* **18**, 444.
Green, D. S., Owano, T. G., Williams, S., Goodwin, D. G., Zare, R. N., and Kruger, C. H. (1993). *Science* **259**, 1726.
Lagerqvist, A., and Miescher, E. (1966). *Can. J. Phys.* **44**, 1525.
Lucht, R. P., Farrow, R. L., and Rakestraw, D. J. (1993). *J. Opt. Soc. Am.* B **9**, 1508.
McCormack, E. F., Pratt, S. T., Dehmer, P. M., and Dehmer, J. L. (1993). *Chem. Phys. Lett.* **211**, 147.
McCormack, E. F., Pratt, S. T., Dehmer, P. M., and Dehmer, J. L. (1994). *Chem. Phys. Lett.* **227**, 656.
McCormack, E. F., Pratt, S. T., Dehmer, P. M., and Dehmer, J. L. (1995). *J. Chem. Phys.* **102**, 4740.
Miescher, E., and Huber, K. P. (1976). *In* 'Spectroscopy, MTP Int. Rev. of Science', Ser. 2 (Ed. D. A. Ramsay), p. 37 (Butterworths: London).
Raoult, M. (1987). *J. Chem. Phys.* **87**, 4736.
Rose, T. S., Wilson, W. L., Wackerle, G., and Fayer, M. D. (1987). *J. Chem. Phys.* **86**, 5370.
Vaccaro, P. H. (1994). *In* 'Molecular Dynamics and Spectroscopy by Stimulated Emission Pumping' (Eds H.-L. Dai and R. W. Fields), p. 1 (World Scientific: Singapore).
Wheeler, M. D., Lambert, I. R., and Ashfold, M. N. R. (1993). *Chem. Phys. Lett.* **211**, 381.
Williams, S., Rahn, L. A., Paul, P. H., Forsman, J. W., and Zare, R. N. (1994*a*). *Opt. Lett.* **19**, 1681.
Williams, S., Tobiason, J. D., Dunlop, J. R., and Rohlfing, E. A. (1995). *J. Chem. Phys.* **102**, 8342.
Williams, S., Zare, R. N., and Rahn, L. A. (1994*b*). *J. Chem. Phys.* **101**, 1072.
Zhang, Q., Kandel, S. A., Wassermann, T. A. W., and Vaccaro, P. H. (1992). *J. Chem. Phys.* **96**, 1640.

Manuscript received 21 April, accepted 18 October 1995